

# Unusual thermal expansion and Curie temperature variation in dhcp-iron hydride under high pressure

Yuichiro Mori, Katsutoshi Aoki, Masahiro Takano, and Hiroyuki Kagi

*Graduate School of Science,  
The University of Tokyo,  
7-3-1 Hongo, Bunkyo-ku, Tokyo 113-0033*

\*

Ina Park

*Center for Computational Quantum Physics (CCQ),  
Flatiron Institute, New York, NY 10010, USA*

Zifan Wang

*Center for High Pressure Science and Technology Advanced Research  
Shanghai 201203, People's Republic of China*

Duck Young Kim

*Center for High Pressure Science and Technology Advanced Research  
Shanghai 201203, People's Republic of China*

*and*

*Division of Advanced Nuclear Engineering,  
Pohang University of Science and Technology  
Pohang 37673, Republic of Korea*

Noriyoshi Tsujino, Sho Kakizawa, and Yuji Higo

*Japan Synchrotron Radiation Institute  
1-1-1 Koto, Sayo, Hyogo 679-5198, Japan*

(Dated: January 16, 2025)

## Abstract

Hydrogen incorporation into iron interstitial sites under high-pressure conditions forms stoichiometric iron monohydride (FeH) with a double hexagonal close-packed (dhcp) structure. This structure is stable over a broad pressure-temperature range, where ferromagnetic-paramagnetic transitions occur. In this study, using synchrotron X-ray diffraction, we identified negative thermal expansion and thermally invariant volume behavior in dhcp-FeH. Our findings, supported by DFT+DMFT calculations, reveal that these thermal effects are governed by magnetic transitions. The Curie temperature decreases linearly with pressure at a rate of  $\sim 21$  K/GPa, reaching 300 K at 28 GPa. Experimentally measured magnetostriction is an order of magnitude smaller than prior theoretical predictions, possibly due to volume expansion induced by hydrogen incorporation.

## INTRODUCTION

Hydrogen atoms occupy the interstitial sites of iron and form iron hydrides by maintaining metallic properties under high-pressure conditions [1]. Dissolved hydrogen atoms expand the interatomic distance and drastically change the physical properties of metallic iron, such as elasticity, magnetism, phase boundaries, and electronic properties through Fe-H electronic interactions [2–6]. The physical properties of iron hydrides attract keen attention as a representative transition metal hydride for understanding the interaction between  $3d$  transition metal and hydrogen atoms. The change in the physical property of iron by hydrogenation is also essential for the Earth and planetary sciences because hydrogen is a promising light-element candidate in the iron core of the rocky planets [7, 8]. Stoichiometric iron hydride (FeH) with double hexagonal close-packed (dhcp) structure is stable in wide pressure and temperature region [5], giving that the hydrogen effect on physical properties will be most pronounced in dhcp-FeH. The dhcp structure is a double periodic structure of hcp that appears only in hydrides. Iron hydride with a dhcp structure is an excellent example for investigating the contribution of interstitial hydrogen to the physical properties of iron. Neutron diffraction [3] and Mössbauer [9] experiments showed that dhcp-FeH exhibits ferromagnetism similar to bcc iron.

The magnetic transition point at high pressure and ambient temperature has been intensely investigated. Mössbauer spectroscopy and X-ray magnetic circular dichroism (XMCD) experiments revealed that the ferromagnetic-paramagnetic transition point of

dhcp-FeH is estimated to be around 30 GPa at room temperature [4, 9–11]. This magnetic behavior is consistent with *ab initio* calculations [12]. Measuring the change in the electrical conductivity associated with the magnetic transition is one of the conventional methods to study the magnetic transition. However, the applications of those experimental approaches to metal hydrides under pressure are limited to low temperatures [13]. Measurements of the elastic wave velocity of FeH [4, 14] showed that the pressure derivative of the body wave changes around 20–40 GPa at 300 K with ferro-paramagnetic transition pressure. Compression measurements suggested that magnetic transition pressure at 300 K ( $P_{tr}$ ) is approximately 30–50 GPa [5, 15]. However, it is difficult to determine the exact magnetic phase transition point due to the gradual decrease in the magnetic moment [11], which is directly related to the ambiguity of phase transition pressures. *Ab initio* density functional theory calculations showed that the magnetic transition pressure is 45–60 GPa at 0 K [12, 16]. However, the experimental clarification of the physical properties of dhcp-FeH at high temperatures has yet to be performed due to technical difficulties. Pressure dependence of magnetic-transition temperature (Curie temperature) of dhcp-FeH was only investigated by CPA [17] and LAPW [18] calculations. Certain ferromagnetic alloys have an anomalously low thermal expansion coefficient due to the cancellation of phonon and magnetic contributions [19]. This invariable thermal expansion, the invar effect, is commonly seen in Fe–Ni and Mn–Ni alloys [20–23]. Spontaneous magnetization causes volume expansion in the invar alloys called magnetostriction. To date, Fe-based Invar alloys are substitutional alloys, such as Fe–Ni and Fe–Co, where the Curie temperature can be tuned by continuously varying the amount of the counterpart metal. On the other hand, magnetostriction behavior (i.e., invariant and negative thermal expansion behavior) in the interstitial alloys has not been reported except cementite [24]. In this study, we investigated the elastic behavior and the effect of magnetism on the elasticity of dhcp-FeH at high temperatures by combining experimental and computational approaches. The pressure and temperature conditions of the ferromagnetic-stable region (*i.e.*, clarification of the pressure dependence of the Curie temperature,  $T_C$ ) were also explored by X-ray diffraction experiments.

## METHODOLOGY

### EXPERIMENTAL PROCEDURE

$P$ - $V$ - $T$  measurements of dhcp-FeH conditions were performed to examine the elastic behavior at high-pressure and high-temperature (HPHT) conditions. *In-situ* energy-dispersive X-ray diffraction experiments under HPHT conditions were carried out at BL04B1, SPring-8 and NE7A, PF-AR, KEK. For the pressure generation, the Kawai-type multi-anvil apparatus was applied to the DIA-type apparatus combined with the uniaxial presses, 'SPEED-Mk.II' [25] and 'MAX-III' installed at BL04B1 and NE7A, PF-AR, respectively. In the cell assembly, the pelletized iron powder and ammonia borane were encased together (the detail of the assembly was summarized in Supplementary Materials [26] and Fig. S1). For phase identification and lattice parameter determination, the X-ray diffraction profiles were analyzed using PDIndexer software [27, 28]. The detailed experimental procedures are as follows. (i) the sample was compressed to 13–15 GPa, in which the hcp phase is the stable region for pure Fe [29]. (ii) the temperature was increased to 850 K to decompose the hydrogen source ( $\text{NH}_3\text{BH}_3$ ) and induce the formation of dhcp-FeH. Time-resolved X-ray diffraction (XRD) measurements were performed every two minutes to monitor the phase transition and the volume expansion by hydrogenation for 80 min (Fig. S2 in the Supplementary Materials [26]). (iii) The time-resolved XRD patterns of dhcp-FeH were obtained by decreasing the temperature from 850 K to 300 K. Each XRD pattern was accumulated for 4 min. The temperature of each profile was determined as the average of the 25 temperature points recorded through the series of time-resolved diffraction measurements. Pressure measurements were carried out before and after the temperature decreasing paths; a linear  $P$ - $T$  relation was estimated to interpolate the pressure at each measurement point. The preliminary experiments confirmed the validity of this exploratory assumption. (See Supplementary Materials [26]). (iv) After a series of XRD measurements at a certain load, the sample was compressed to the subsequent target pressure. (v) The sample was heated to the maximum temperature we applied and returned to the process (iii) and repeated (iii)–(v) three times additionally.

## COMPUTATIONAL DETAILS

First-principles density functional theory plus dynamical mean-field theory (DFT+DMFT) calculation was performed to investigate the FM and PM states of dhcp-FeH at various *HPHT* conditions. The implementation of DMFT [30, 31] enables not only approaching the finite temperature conditions but also treating the electronic correlation effect of Fe *d* electrons by describing dynamical quantum fluctuation, in which the latter is revealed to be significant for *dual* (itinerant-versus-localized) nature of magnetic iron [32]. There were also previous studies [33–36] that pointed out that the electronic correlation effects could be non-negligible at high temperature and/or high pressure conditions. The crystal structure information - unit cell volume at each pressure condition and  $c/a$  ratio - were adopted from the experimental reports [15]. Those values are tabulated in the supplementary material, Table S1, and a constant  $c/a = 3.270$  was used for the pressure range investigated via DFT+DMFT. The charge self-consistent DFT+DMFT calculation was performed as implemented in the DFT + embedded DMFT Functional (eDMFT) code [37]. The DFT calculation with full-potential augmented plane wave method was performed by using WIEN2k code [38], where the Perdew-Burke-Ernzerhof (PBE) generalized gradient approximation (GGA) was used for the exchange-correlation functional [39]. A  $19 \times 19 \times 5$   $k$ -point mesh was used for the electronic self-consistent calculation. For DMFT part, the hybridization energy window ranges from -10 eV to 10 eV for the case of  $P = 4$  GPa condition, and the corresponding band indices range were fixed for higher pressure conditions. Slater parametrization with Coulomb interaction parameter  $U = 5.7$  eV and Hund's exchange interaction parameter  $J = 0.8$  eV were used, which was used for Fe  $3d$  orbitals [40]. The impurity model was solved by using a continuous-time quantum Monte Carlo (CTQMC) impurity solver [37, 41]. The equations of states were calculated using Vienna *ab initio* simulation package (VASP). We used the GGA of PBE for the exchange-correlation functional with the cut-off energy of 800 eV. Monkhorst-Pack  $k$ -point mesh with  $0.03(2\pi/\text{\AA})$  mesh resolution was used. We conducted the PBE+ $U$  calculations to account for the correlated  $d$  orbitals of Mn and  $U_{\text{eff}} = U - J$  was chosen to 0 – 7 eV to investigate the Coulomb correlation effect on the equations of states.

## RESULTS AND DISCUSSION

Figure 1 portrays the  $T$ - $V$  relations of dhcp-FeH obtained by *in-situ* XRD measurements at each pressure path. The unit-cell volumes of dhcp-FeH were almost constant below 500 K at the lowest-pressure path (the topmost  $T$ - $V$  curve of Fig. 1). At higher pressures, the  $T$ - $V$  curves of dhcp-FeH kinked. These kinks became sharper as the pressure increased. The remarkable  $T$ - $V$  behavior of dhcp-FeH can be explained by the competition between the magnetostriction and thermal expansion effects. The temperature-independent behavior of the unit-cell volume at the lowest pressure can be interpreted as the result of the cancellation of both effects. The appearance and sharpening of the kink can be explained by the predomination of the magnetostriction effect with increasing pressure. First, the magnetic properties of dhcp-FeH were assessed by using the experimentally determined  $T_C$  from the minima of the  $T$ - $V$  curve combined with previous experimental works. The magnetic moment of iron of dhcp-FeH was determined by neutron diffraction at  $P = 4.2$  GPa and 300 K [42]. On the other hand, the pressure dependence of the magnetic moment at room temperature was clarified up to  $P \sim 30$  GPa. Combining these results with the simple mean field approximation of  $S = 1/2$ , the spontaneous magnetization ( $M_S$ ) can be determined from  $T/T_C$ . Figure S3(a) shows the  $M_S$  at experimental points below  $T_C$ . Spontaneous magnetization ( $M_S$ ) just below  $T_C$  is described as proportional to  $M_S \propto (T_C - T)^\beta$ , in which  $\beta$  is one of the critical index with universality. In the classical view, such as the Ginzburg-Landau theory and the mean (molecular) field approximation,  $\beta$  equals 0.5 near  $T_C$ . Here,  $M_S$ - $T/T_C$  relation is described to  $T/T_C \sim 0.6$ , which exceeds ‘the vicinity’, and the modeled slope is slightly deviated from 0.5. Typically, experimental values of  $\beta$  are around 0.33 [43], close to 0.365 for the three-dimensional Ising model and 0.325 for the three-dimensional Heisenberg model. In these models, spin fluctuations due to short-range correlations are taken into account, in contrast to the spin-fluctuation free molecular field approximation. Magnetostriction is proportional to the square of the spontaneous magnetization both experimentally and theoretically [44, 45]. Thus, using  $\Delta V_M/V \propto M_S^2$ , we obtained  $\beta$  for dhcp FeH from the  $\Delta V_M$ - $T/T_C$  (Fig. S3(b)). They range from 0.39 to 0.47 and 80–90% of the first estimation (Fig. S3(a)), indicating that the  $\Delta V_M$ - $T/T_C$  curves are interpreted as a ferromagnetic-paramagnetic transition with small spin fluctuations.

Additional DFT+DMFT calculation at  $P = 29$  GPa exhibited small but finite value of

$M_S = 0.2 \mu\text{B}$  at  $T = 58 \text{ K}$  (Fig. S5), and the scaled  $T_C$  (Details provided in Supplementary Materials [26] and Fig. S5) was obtained as 258 K. It also follows the linear  $P$ - $T_C$  relation, and simple extrapolation estimates  $P_{\text{tr}}$  to around 41 GPa at  $T = 0 \text{ K}$ . On the other hand, deviation from the Ginzburg–Landau critical behavior and significant fluctuation of magnetization would imply that  $P = 29 \text{ GPa}$  could be already near the ferromagnetic-paramagnetic phase boundary at low temperature conditions.

During the descending temperature process, the volume expansion induced by ferromagnetism increases the unit-cell volume at the magnetic transition boundary. Thus, the bending point of the  $T$ - $V$  curves on Fig. 1 corresponds to the Curie temperature ( $T_C$ ). The details on the accurate estimation of  $T_C$  from the  $T$ - $V$  curves are provided in the Supplementary Materials [26]. The pressure dependence of  $T_C$  combined with the calculated results is shown in Fig. 2. The  $T_C$  of dhcp-FeH decreased linearly with pressure ( $R^2 = 0.92$ ). By extrapolating the linear  $P$ - $T_C$  to ambient pressure, the  $T_C$  of dhcp-FeH was estimated to be 940 K at 0 GPa. The estimated  $T_C$  is close to that of bcc-Fe, 1053 K. This linear  $P$ - $T_C$  relation is compared to DFT+DMFT calculation results. First, in Fig. 2(a),  $P$ - $T$ - $M$  obtained from DFT+DMFT calculation is shown. We note that, since DFT+DMFT with density-density type of Coulomb interaction form usually overestimates the Curie temperature by factor or 2 to 3, while giving the reasonable value of magnetization [33, 40], scaled temperature axis was used for this figure to directly compare with experimental values (triangles). Fig. S4(b) in Supplementary Materials [26] portrays the further details of temperature scaling. In our calculation, the Curie temperature was overestimated by factor of around 2.2, *i.e.*, the temperature axis is scaled by the factor of  $\sim 0.46$ .

From DFT+DMFT calculation, the magnetic moment is almost saturated at  $P = 4 \text{ GPa}$  and  $T = 116 \text{ K}$ , and it is revealed  $M_S \sim 2.06 \mu\text{B}/\text{Fe-atom}$ . This value is close to that of bcc-Fe, 2.218  $\mu\text{B}/\text{Fe-atom}$  at 0 K and 0.1 GPa, considering the higher-pressure conditions. The resultant  $T_C$  and magnetic moment of dhcp-FeH are consistent with the previous DFT calculations and ND experiments [16, 42]. Saitoh et al. (2020) [42] suggested that bcc-Fe and dhcp-FeH have similar  $T_C$  because of the comparable magnetic moments. The obtained  $M_S$  and  $T_C$  of dhcp-FeH are consistent with those of bcc-Fe, indicating the validity of the above explanation. Then, the temperature condition at which the magnetization becomes zero is defined as  $T_C$  (as marked with arrows in Fig. S4(b)), and it shows consistent slope of the linear  $P$ - $T_C$  relation compared to the experimental results, as shown in Fig. 2(b). The



$P_{\text{tr}}$  determined in this study is approximately 27 GPa at room temperature, and it is close to the previous estimated value,  $P_{\text{tr}} = 30$  GPa by XMCD and Mössbauer measurements. Figure S5 shows the relation between pressure and magnetization at the lowest temperature condition considered in DFT+DMFT calculation (Fig. S5 shows the magnetization at lowest pressure). It is also consistent with the reported  $P_{\text{tr}}$  value. The substantial decrease in  $T_C$  with  $P$  is also demonstrated by the  $V$ - $P$  curves in Fig. S6 of the Supplementary Materials [26]. In the paramagnetic region, the  $T$ - $V$  relation was postulated to be linear. Then, the paramagnetic  $V$  in the ferromagnetic region can be estimated from the extrapolated this linear relation to the lower temperature regions (the ferromagnetic region). By subtracting those hypothetical  $V$  of the paramagnetic state from the observed  $V$ , we can make an estimate of the magnetostriction. Let  $V_M$  denote the difference in volume between them (i.e.,  $\Delta V_M = V_{\text{ferromag.}}^{\text{obs.}} - V_{\text{paramag.}}^{\text{est.}}$ ). Figure 3 shows the variation of  $\Delta V_M$  with a normalized temperature of  $T/T_C$ . The  $\Delta V_M$ - $T/T_C$  curves overlap within the experimental errors and the relation between  $T/T_C$  and  $\Delta V_M$  is consistent and independent on pressure (Fig. 3). Note that the slope of  $T$ - $\Delta V_M$  becomes steeper at higher pressures as  $T_C$  decreases with pressure. It can be clearly seen by changing from the horizontal axis,  $T/T_C$ , in Fig. 3 to  $T$ . This finding suggests that magneto-volume coupling is stronger at higher pressures.

From DFT+DMFT calculations, magnetic moment,  $M_S$  at  $T/T_C \sim 0$  are approximately 1.2 and 1.4 times of those at  $T/T_C \sim 0.5$  at 15 and 21 GPa, respectively (Fig. 2). Since it has been found from experiments that the obtained  $\Delta V_M$  is  $0.5 \text{ \AA}^3$  at  $T/T_C \sim 0.5$  (Fig. 2), the value of  $\Delta V_M^0$  becomes  $0.7 \text{ \AA}^3$  at 15 GPa and  $1.0 \text{ \AA}^3$  at 21 GPa, respectively. The resulting value of  $\Delta V_M^0$ ,  $0.7$ – $1.0 \text{ \AA}^3$ , is significantly smaller than the previously calculated estimates of  $4.0 \text{ \AA}^3$  [1, 12], and it is even  $\sim 1/10$  of the hydrogen-induced volume expansions in Fe hydrides. Here, the volume expansions of 20 to  $2.5 \text{ \AA}^3$  per H(D) atom for fcc and hcp Fe hydride/deuteride [46–49] were converted to  $8$ – $10 \text{ \AA}^3$  per dhcp unit-cell containing four Fe atoms. The very small magnetostriction is synonymous with the difference between ferromagnetic and paramagnetic  $V_0$  being smaller than previously predicted by theory. This indicates that the volume expansion due to hydrogenation has already sufficiently increased the Fe–Fe distance and that structural stabilization can be achieved even if the repulsive force due to magnetostriction is small. Schematic of this interpretation is shown in Fig. S7.

To evaluate  $\Delta V_M^0$ , we also constructed an equation of state for paramagnetic dhcp-FeH by the previous results of compression studies at 300 K [5, 15]. We derived the equation of states

of paramagnetic dhcp-FeH by refitting those datasets at  $P \geq 60$  GPa, which is well above the magnetic transition pressure. The pressure derivative of  $K_0$  ( $K'_0$ ) is assumed to be 4. By applying the dataset to Vinet Equation of States,  $V_0$  and  $K_0$  are  $54.3(5) \text{ \AA}^3$  and  $165(9)$  GPa, respectively. The estimated  $V_0$  of paramagnetic dhcp-FeH has a significantly large value compared to the theoretically predicted one, which ranges from  $50$  to  $51 \text{ \AA}^3$  at  $300 \text{ K}$  [5, 12]. The difference in  $V_0$  is probably due to the fitting using only high-pressure volume data above  $50$  GPa and the lack of low-pressure volume data required to determine an accurate  $V_0$ . One of the previous compression studies reported an equation of state well reproducing the theoretically predicted  $V_0$  using  $K'_0 = 8.5(29)$ , twice the usual value of  $K'_0 = 4$  [15]. We also constructed equations of states (EoS) of ferromagnetic and paramagnetic dhcp-FeH by LDA and GGA calculations using different  $U$  values were carried out (Fig. S8 in Supplementary Materials). Equilibrium volumes with varying  $U$  parameters are shown in Table. S2. We can reproduce small  $\Delta V_M = 3.02 \text{ \AA}^3$  for LDA and  $5.6 \text{ \AA}^3$  for GGA per unit cell by adopting small  $U = 1 \text{ eV}$ . The value,  $U$  is an empirical value, but related to the balance of itinerant and localized electron. In dhcp-FeH, we can reproduce small  $V_M$  by adopting small  $U$ , suggesting that the  $d$ -orbital electrons of iron are itinerant and not localized.

## CONCLUSIONS

In this study, we first revealed the magnetoelastic behavior of dhcp-FeH and determined the pressure dependence of Curie temperature. The concept of this experimental method is to apply the thermal expansion measurement experiment, which is a standard method to explore the invar behavior, to high pressure. As a result, although measuring the absolute value of thermal expansion was difficult, we established a technical method to capture magnetostriction and revealed the invar and negative thermal expansion behavior of dhcp-FeH at high pressures. Combined with DFT and DMFT calculations, profound insight into the quantification of the interaction between elasticity and magnetism was offered. Recently, DFT+DMFT calculations has been promoted and applied to ferromagnetic metals such as bcc-Fe [40, 50, 51] and hcp-Fe [52]. This study is the first report for the DFT+DMFT approach to determining the magnetic properties of dhcp-FeH in various  $PT$  conditions. The detailed description of the magneto-volume effect is critical to not only about the physical

properties of metal hydrides, but also about the picture of the magnetic transition and its elastic effects. The method in this study is also applicable to estimate  $T_C$  for ferromagnetic materials under high pressure. Our result also showed the perspective that dhcp-FeH is a good target for establishing the validity of the calculation method because dhcp-FeH is ferromagnetic over a wide pressure (volume) range while the crystal structure is unchanged.

The work by the authors described in this paper was supported by a Grant-in-Aid for Encouragement of Research Fellows (22J21462) to Y.M. and a JSPS Grant-in-Aid for Scientific Research (23H00140) to H.K. SRXRD experiments were conducted at BL04B1, SPring-8 (project numbers: 2023B0314, 2024A0314 to Y.M. and 2022A1319, 2022A2067, 2022B2118, 2023A1250 to S.K.) and NE7, PF-AR, and KEK (project numbers: 2023G668 to H.K.). Y.M. designed this study and Y.M. and K.A. made conceptualization. Y.M. carried the statistical processing using the obtained data. I.P. conducted DFT+DMFT calculations, and I.P. and D.K. analyzed the results. Z.W. and K.M. carried out DFT calculations to derive thermal equation of state. Y.M., M.T., and K.H. carried out some preliminary experiments at PF-AR NE7 KEK. Y.M., M.T., K.H. carried out *in-situ* X-ray diffraction experiments at BL04B1, SPring-8. S.K, N.T and Y.H. supported the experiments at BL04B1, SPring-8. All authors read and approved the final manuscript. I.P. and D.K. acknowledge J.S. for fruitful discussion. I.P. acknowledges J.K. and H.C. for fruitful discussion.

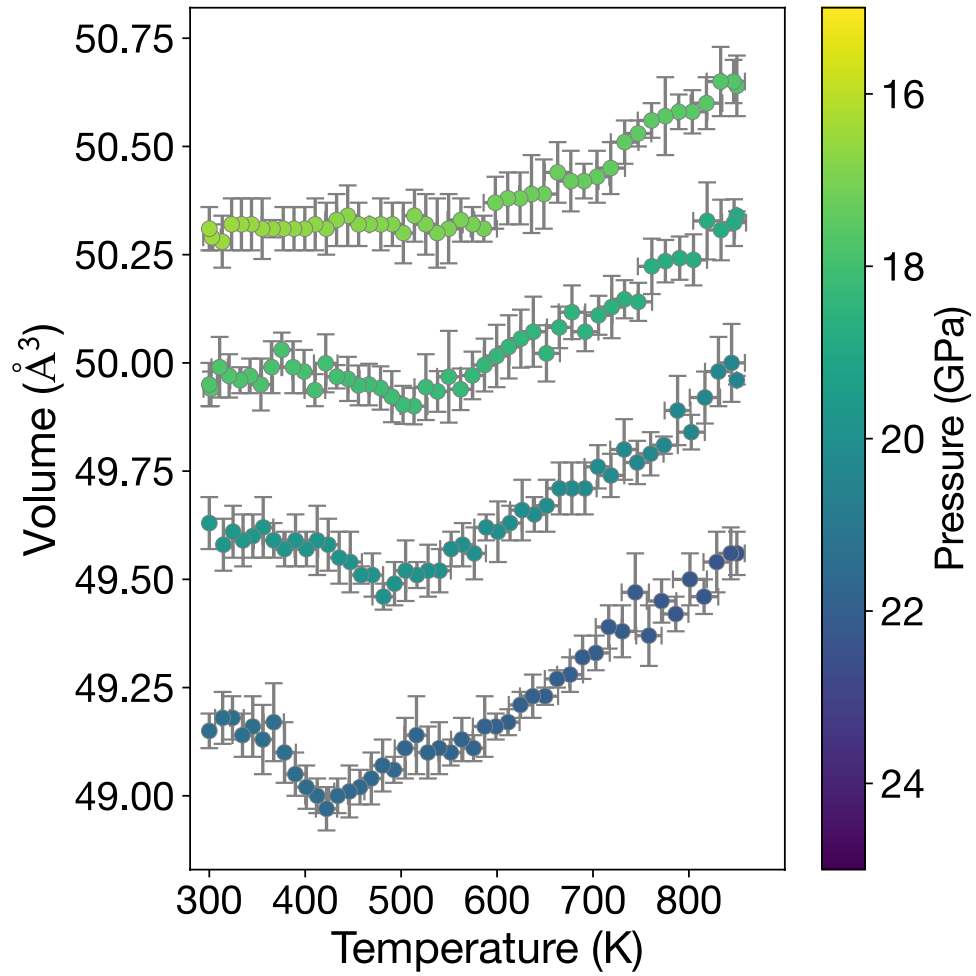


FIG. 1. Temperature v.s. Unit-cell volume of dhcp-FeH. Color scale also shows the pressure. All data points were obtained in the temperature-decrease pathway.

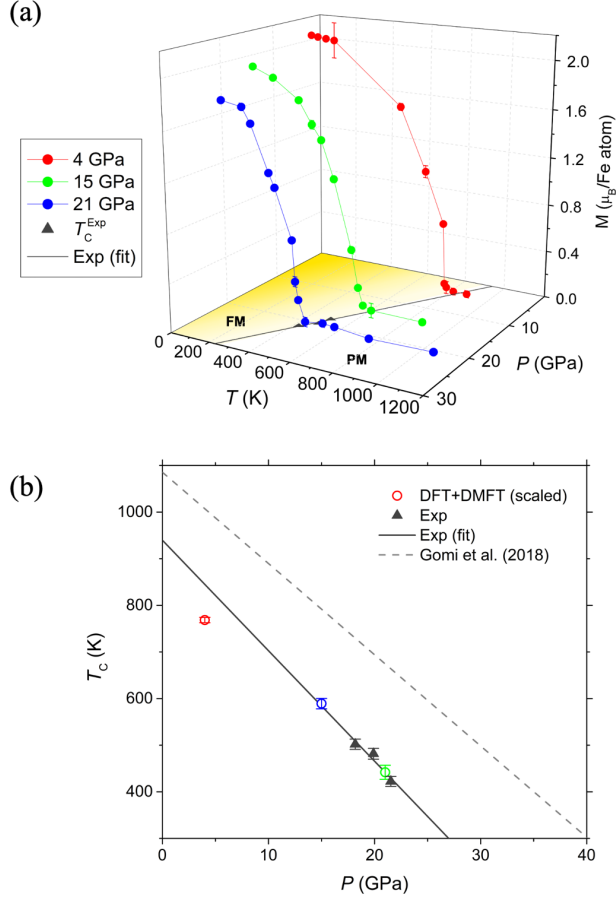


FIG. 2.  $P$ - $T$ - $M$  of dhcp-FeH obtained from DFT+DMFT calculation. Dots are magnetization,  $M$ , as a function of the scaled temperature (refer supplemental material) at  $P = 4$  (red), 15 (green), and 21 (blue) GPa. Triangles are experimentally determined Curie temperature,  $T_C$  and solid line is the linear fit of the experimental values as a function of pressure. (b)  $P$ - $T_C$  of dhcp-FeH from DFT+DMFT calculation (circle) and  $T$ - $V$  experiment (triangle) in this work, and Korringa-Kohn-Rostoker method with coherent potential approximation (KKR-CPA) calculation (dashed line) [17] Triangles are  $T_C$  measured in experiment, and solid line is the linear ferromagnetic-paramagnetic boundaries of each path are determined by fitting the  $T$ - $V$  of the high temperature part (ferromagnetic part) as a linear function of temperature and interpolated to lower temperature to obtain  $T_C$ . The error bars on the vertical axis represent the temperature change during one measurement, while the error bars on the horizontal axis represent the expected pressure change for each measurement. The calculated  $P$ - $T_C$  relation is normalized (the detail of normalization process is described in Supplementary Materials).

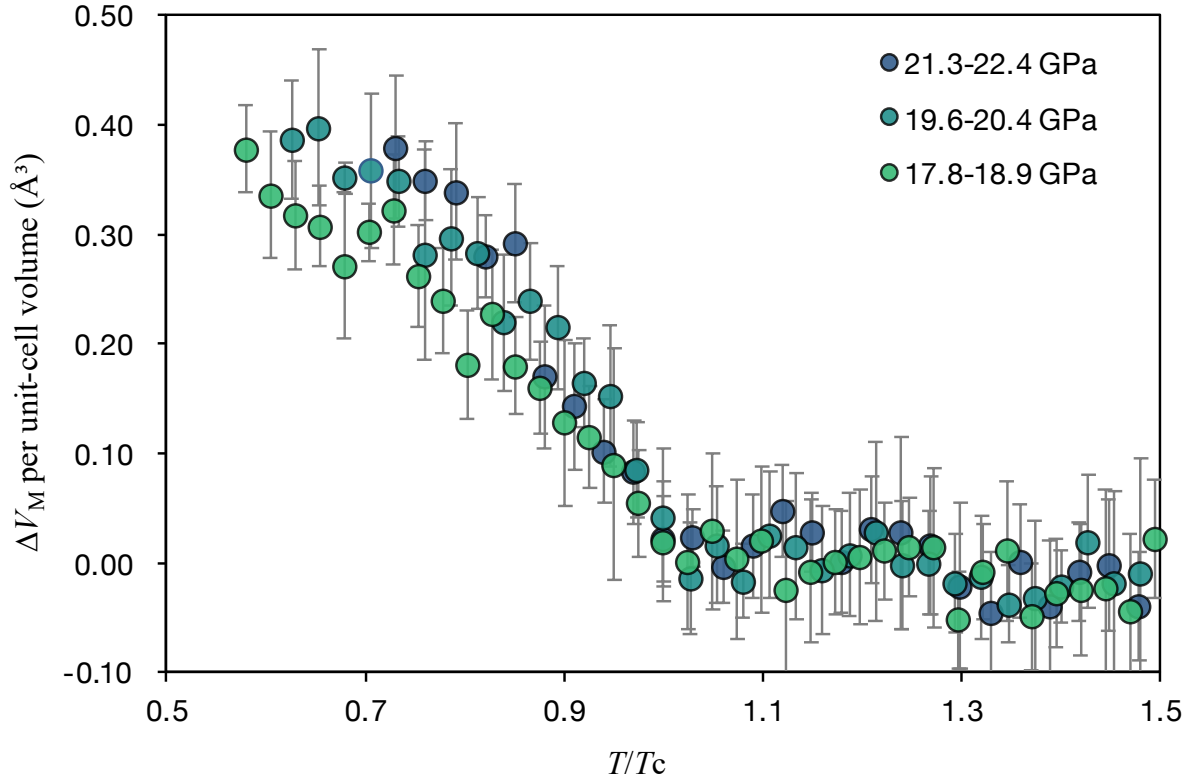


FIG. 3. Temperature dependence on Volume expansion induced by ferromagnetism ( $\Delta V_M$ ). Temperature was normalized by  $T_C$  of each path.

## SUPPLEMENTARY MATERIALS

### PRESSURE DETERMINATION

$P$ - $T$  paths depend on the material of the sample assemblies, the temperature range, and the heating itinerary. It should be noted that, the pressure decreases almost linearly from the pressure before and after each temperature-decreasing path evident from the preliminary experiment, which measured every 50 K and 100 K with the same assembly and the same pressure regions. We succeed in obtaining ‘snapshot-like’ XRD by slowly cooling during time-resolve XRD measurements. Temperature change during each measurement, 4 min is about less than 15 K, and pressure change is less than 0.05 GPa by applying the  $P$ - $T$  linear approximation.

### CURIE TEMPERATURE ( $T_C$ ) DETERMINATION

For the determination of  $T_C$ , the temperature at  $P$ ,  $T$ , where the minimum value of the volume in the  $T$ - $V$  path was taken, was taken as  $T_C(P)$ , as negative thermal expansion behavior was observed at the three paths on the high-pressure side. On the other hand, the lowest pressure path showed invar behavior and it was difficult to precisely determine a significant minimum volume value beyond the error range. In these areas, coupled with the large unit-cell volume error, the determination of the magnetic boundary can be arbitrary. Therefore, the lowest pressure path with portraying the invar behavior was excluded for  $T_C$  determination.

### THE DETAILS OF THE CELL ASSEMBLY

In the cell assembly, Fe pellet mixed with hexagonal BN as a grain-growth inhibitor [53] and a hydrogen source, ammonia borane ( $\text{NH}_3\text{BH}_3$ ) [54, 55], were loaded into the NaCl capsule. It is empirically known that 2/3 of the prepared H/Fe ratio is used to hydrogenate the sample. To make ideally stoichiometric dhcp-FeH, the starting H/Fe ratio was set to 2, giving that the molar content of released hydrogen was predicted to be 1.3 times larger than that of iron where hydrogen content is in excess. Pressure and temperature were respectively determined using the pressure marker made of NaCl mixed with MgO grain-growth inhibitor

just below the NaCl capsule and a pair of W3%Re-W25%Re thermocouples. Pressure was determined using the EoS of NaCl [56]. A cylindrical TiB<sub>2</sub> + BN + AlN (EBN, Denka) heater were used. Figure S1 in the Supplementary Materials [26] shows the details of the cell assembly. The sample heating is accomplished by the changing the input electrical power and the temperature was monitored by emf of the inserted thermocouple. By decreasing the applied electrical power, corresponding to 850 K, to 0 W for 180 min and the XRD profile of dhcp-FeH were sequentially obtained during decreasing temperature.

### CRYSTAL STRUCTURE USED IN DFT+DMFT CALCULATION

In DFT+DMFT calculation, the unit cell volume at each pressure condition listed in Table S1 is fixed for the whole temperature range of calculation.

### TEMPERATURE SCALING IN DFT+DMFT CALCULATION

As mentioned in the main text, DFT+DMFT could usually overestimate the value of Curie temperature, and the degree of overestimation depends on the type of Coulombic interaction form. In this calculation, we used so-called 'Ising-type', which only includes the density-density type of interaction. It usually gives two or three times larger Curie temperature, which also can depend on the value of interaction parameters  $U$  and  $J_H$ . Given that overestimation, to compare DFT+DMFT results with experimentally determined values, we first linear-fit the  $P$ - $T_C$  of experimental values and obtained the relation  $T_C^{Exp,estimated}(K) = -21.62P + 896.79$ . Then the temperature scaling factor  $r$  is defined as the ratio between the  $T_C^{DMFT}$  and  $T_C^{Exp,estimated}$  at  $P = 21$  GPa (to avoid the extrapolation). The scaling factor was estimated as  $r \sim 0.458$ . Other pressure conditions were also tested, and the scaling factor  $r$  was between 0.44–0.48. The DFT+DMFT results in the main figure are plotted as a function of this scaled temperature,  $rT$ .



## SUPPLEMENTARY FIGURES AND TABLES

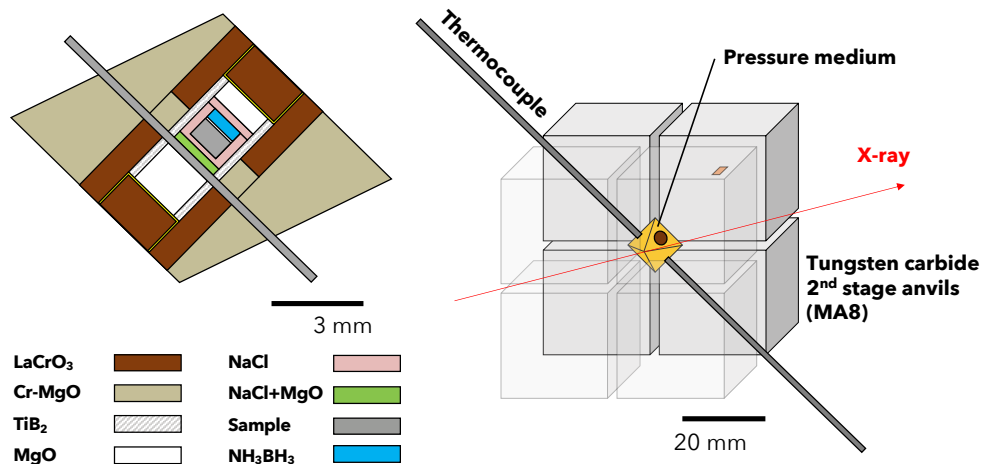


FIG. S1. Cell assembly of XRD measurements under high pressure. Octahedron pressure medium with 10 mm edge length was set into the MA8 (right-hand side of the figure) and compressed by the six first-stage anvils attached to DIA-type guide-block. The temperature was recorded every 10 s by a digital multi-meter of the electromotive force between a pair of the thermocouple inserted nearby the sample capsule.

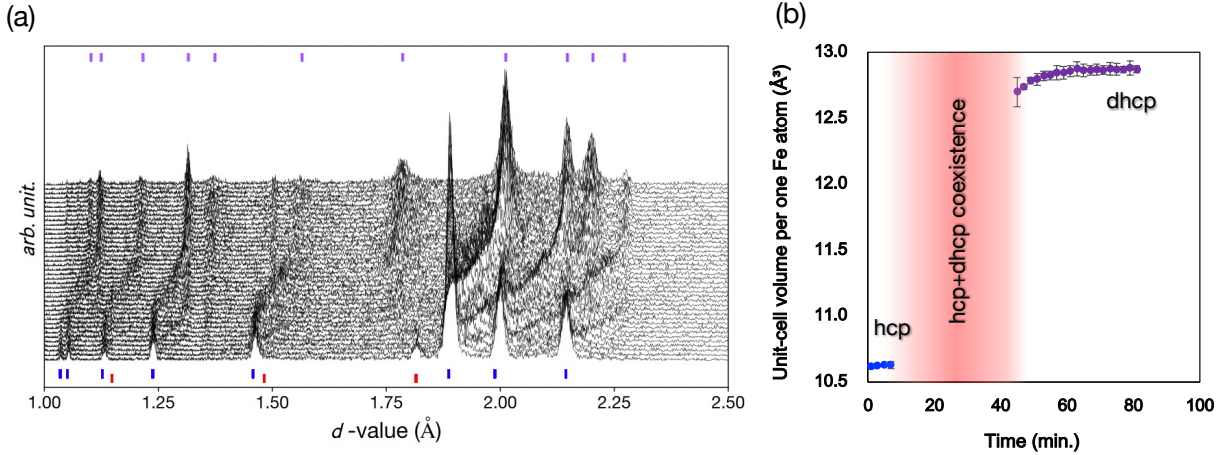


FIG. S2. (a) Hydrogenation of Fe at 15 GPa and 900 K. From bottom to top, hcp iron transform into dhcp structure by hydrogenation. The exposure time of each profile is 120 sec. It took around 80 min until the volume expansion induced by hydrogenation cease. Lower red and blue ticks represent the peaks from surrounding NaCl and hcp-FeH<sub>x</sub>, respectively. Upper purple ticks represent the peaks from dhcp-FeH. (b) Time-resolved unit-cell volume change of iron hydride. In the initial stages of the reaction, hcp-structured FeH<sub>x</sub> is formed. Later, as the hydrogenation FeH<sub>x</sub> reaction proceeds, hydrogen content in the system exceed the solubility of hcp-FeH<sub>x</sub> and dhcp-FeH<sub>x</sub> emerges in addition to the saturated hcp-FeH<sub>x</sub>. In the final stage, hcp-FeH<sub>x</sub> vanished and volume expansion of dhcp-FeH<sub>x</sub> ceased when hydrogen content in iron got saturated

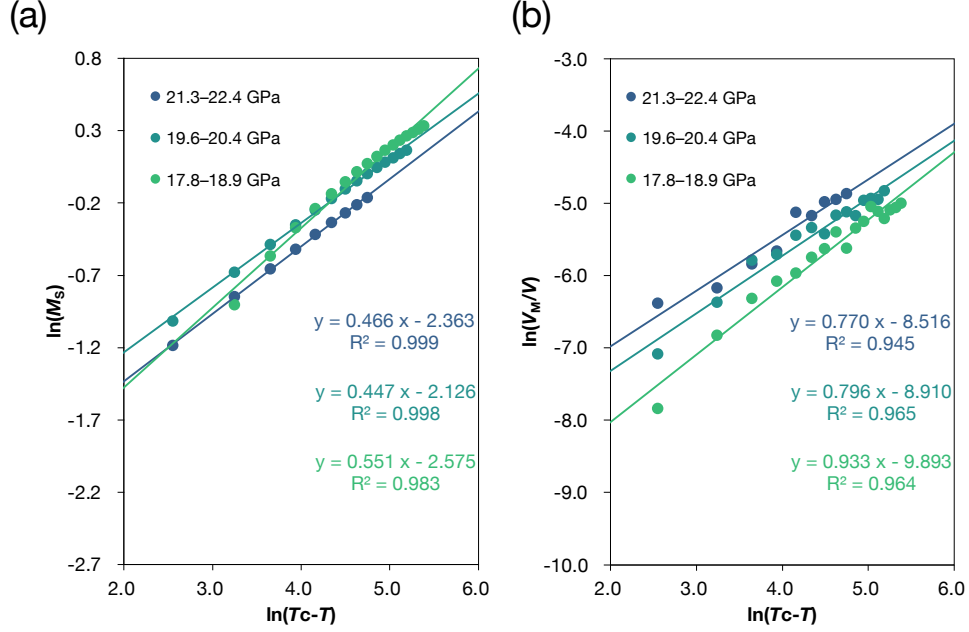


FIG. S3. The critical index estimated from (a) the experimentally obtained  $T_C$  and mean-field approximation and (b) the experimentally obtained  $V_M$  and the relation between spontaneous volume magnetostriction and spontaneous magnetization: (a) The relation between  $M_S$  and  $T/T_C$  of each path.  $M_S$  at room temperature was estimated using the pressure dependence of magnetic moment of Fe in dhcp-FeH clarified by the previous studies [[11, 42] and mean-field approximation with  $S = 1/2$ . The slope is corresponding to the critical index,  $\beta$ . (b) The relation between  $\Delta V_M$  and  $T/T_C$  of each path. The spontaneous volume magnetostriction ( $\Delta V_M/V$ ) is proportional to the square of the spontaneous magnetization ( $M_S$ ) [44, 45] The slope of these plots corresponds to  $2\beta$ .

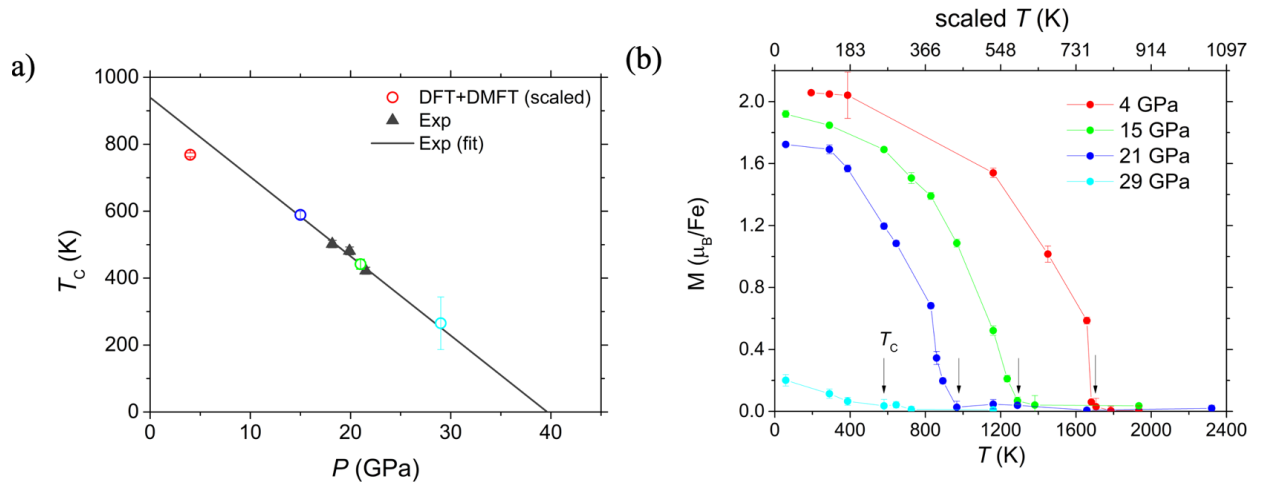


FIG. S4. DFT+DMFT calculation results extended with additional pressure condition of  $P = 29$  GPa. (a)  $T_C$  versus  $P$ . (b)  $M$  versus  $T$ . The bottom-X axis shows raw temperature values used in the DFT+DMFT calculation, and the top-X axis shows the scaled temperature,  $rT$ , used in the main text. The arrow marks the Curie temperature  $T_C$  at which the magnetization becomes zero. Error bars are the standard deviation of the magnetization from the converged Monte Carlo calculation results.

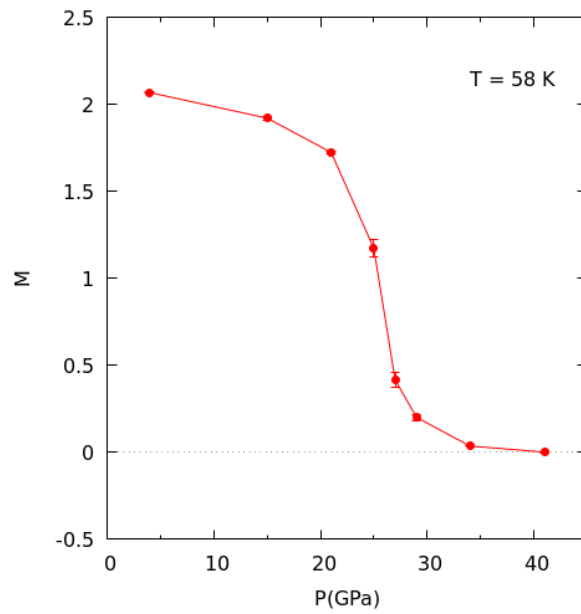


FIG. S5.  $M$  ( $\mu_B/\text{Fe}$ ) versus  $P$ . The temperature condition is  $T = 58$  K except for  $P = 4$  GPa. For  $P = 4$  GPa,  $T = 116$  K was used, at which the magnetization was saturated.

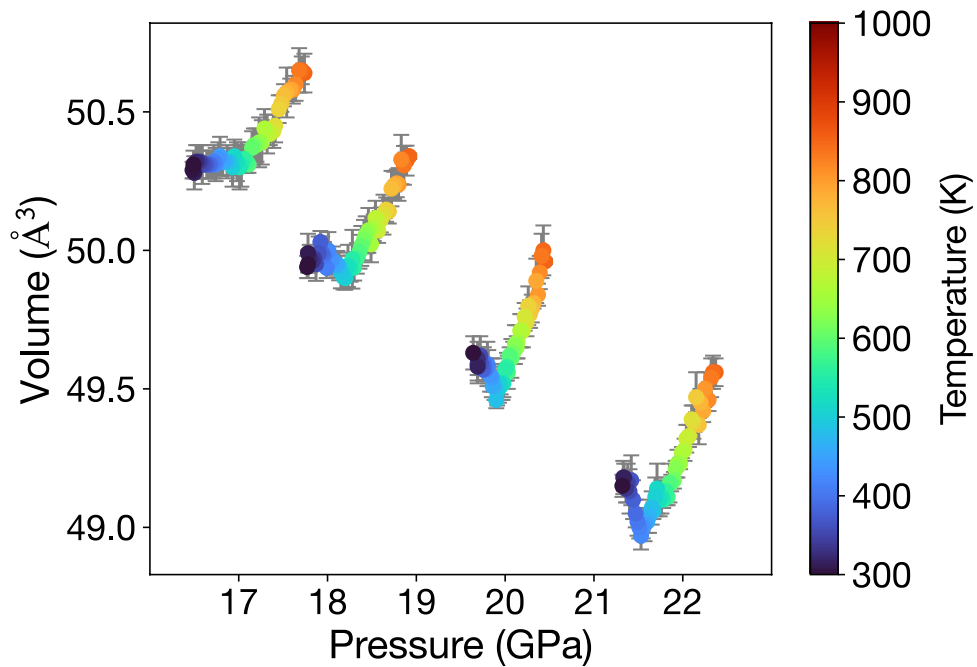


FIG. S6. Pressure v.s. Unit-cell volume of dhcp-FeH. Color scale on the right-hand side shows the temperature. Pressure was derived by the interpolation of linear  $P$ - $T$  in each path. All data points (unit-cell volume of dhcp-FeH) were obtained in the temperature-decrease pathway.

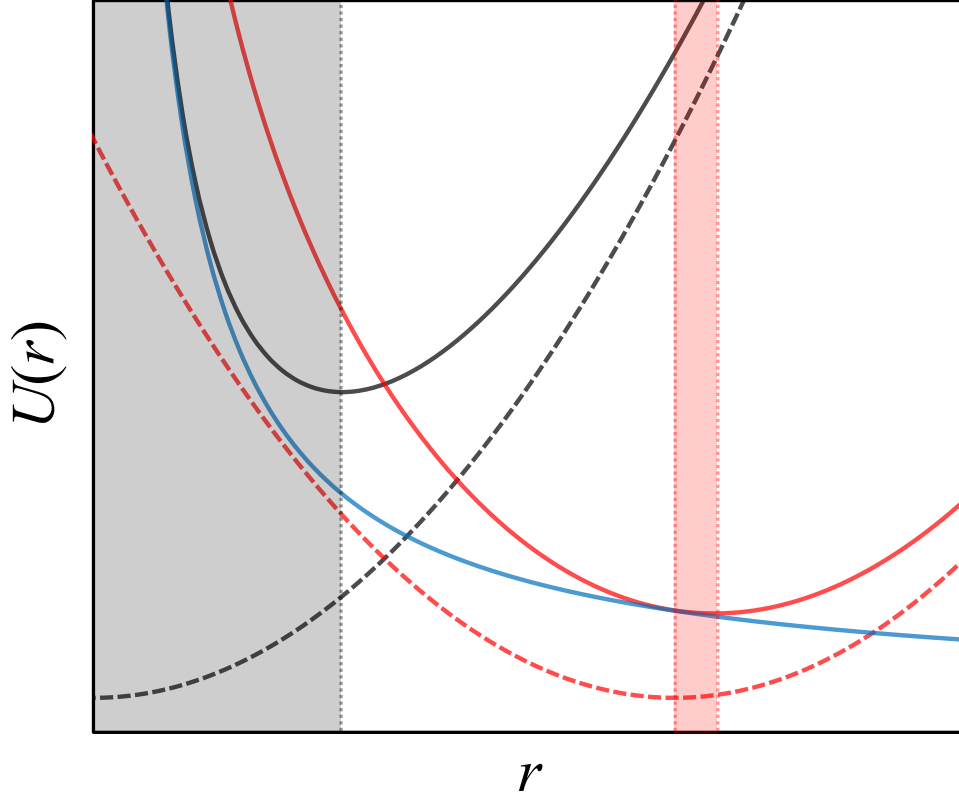


FIG. S7. Schematic drawing to explain the qualitative hypothesis for the very small magnetostriction of iron hydrides. The black dashed line represents the typical relation of potential energy and atomic distance. When the magnetic effect due to ferromagnetism (magnetostriction) occurs, the atomic distance dependence on the potential energy shifts to the black solid line. Note that the magnetic potential (blue solid line) was assumed to be a simple Coulomb repulsion expression. Hydrogenation increases the atomic distance of Fe–Fe, and the minimum potential energy shifts toward a long atomic distance, as shown in the red dashed line. Also, in this case, the magnetic effect changes the energy to the red solid line. Compared to the obtained minimum of each potential, the magnetostriction of already expanded material (red shaded area) is smaller than that of not-expanded material (black shaded area).

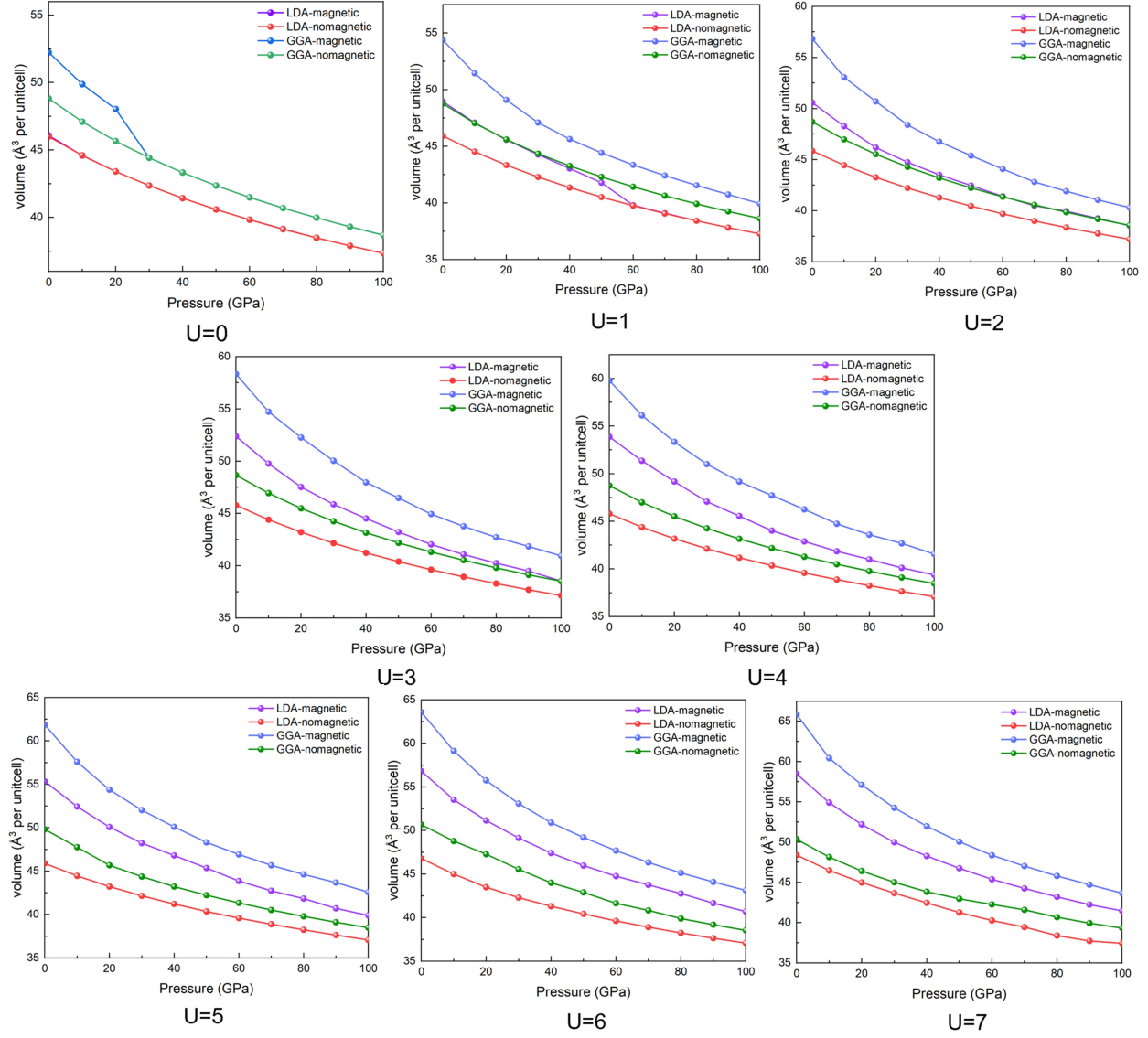


FIG. S8. Equations of states (EoS) of ferromagnetic and paramagnetic dhcp-FeH using LDA and GGA functionals.

TABLE. S1. Crystal structure of dhcp-Fe used in DFT+DMFT calculation. The unit cell volume  $V$  is directly obtained from the reference [15], and the  $c/a$  ratio is 3.270.

$P$ (GPa)	$V$ ( $\text{\AA}^3$ )	$a$ -axis ( $\text{\AA}$ )
4	53.78	2.668
15	50.35	2.610
21	48.86	2.584
29	47.24	2.555

TABLE. S2. Equilibrium  $V_0(\text{\AA}^3)$  with various  $U$  parameters using different pseudopotentials, containing four FeH units.

	LDA-magnetic	LDA-nomagnetic	GGA-magnetic	GGA-nomagnetic
U=0	46.07	45.99	52.23	48.82
U=1	48.94	45.92	54.36	48.76
U=2	50.58	45.85	56.83	48.69
U=3	52.37	45.79	58.33	48.66
U=4	53.88	45.80	59.78	48.75
U=5	55.34	45.89	61.86	49.81
U=6	56.81	46.28	63.58	49.67
U=7	58.48	48.40	65.87	50.36



---

\* Contact author: mory@eqchem.s.u-tokyo.ac.jp

- [1] Y. Fukai, *The metal-hydrogen system: basic bulk properties* (Springer Science & Business Media, 2006).
- [2] C. Elsässer, J. Zhu, S. G. Louie, M. Fähnle, and C. T. Chan, Ab initio study of iron and iron hydride: I. Cohesion, magnetism and electronic structure of cubic Fe and FeH, *Journal of Physics: Condensed Matter* **10**, 5081 (1998).
- [3] V. Antonov, I. Belash, and E. Ponyatovsky, TP phase diagram of the Fe–H system at temperatures to 450°C and pressures to 6.7 GPa, *Scripta Metallurgica* **16**, 203 (1982).
- [4] W. L. Mao, W. Sturhahn, D. L. Heinz, H.-K. Mao, J. Shu, and R. J. Hemley, Nuclear resonant X-ray scattering of iron hydride at high pressure, *Geophysical Research Letters* **31** (2004).
- [5] C. M. Pépin, A. Dewaele, G. Geneste, P. Loubeyre, and M. Mezouar, New iron hydrides under high pressure, *Physical Review Letters* **113**, 265504 (2014).
- [6] T. Meier, F. Trybel, S. Khandarkhaeva, G. Steinle-Neumann, S. Chariton, T. Fedotenko, S. Petitgirard, M. Hanfland, K. Glazyrin, N. Dubrovinskaia, and L. Dubrovinsky, Pressure-induced hydrogen-hydrogen interaction in metallic FeH revealed by NMR, *Physical Review X* **9**, 031008 (2019).
- [7] Y. Fukai, The iron–water reaction and the evolution of the Earth, *Nature* **308**, 174 (1984).
- [8] J. Badding, R. Hemley, and H. Mao, High-pressure chemistry of hydrogen in metals: In situ study of iron hydride, *Science* **253**, 421 (1991).
- [9] I. Choe, R. Ingalls, J. Brown, Y. Sato-Sorensen, and R. Mills, Mössbauer studies of iron hydride at high pressure, *Physical Review B* **44**, 1 (1991).
- [10] T. Mitsui and N. Hirao, Ultrahigh-pressure study on the magnetic state of iron hydride using an energy domain synchrotron radiation  $^{57}\text{Fe}$  Mössbauer spectrometer, *MRS Online Proceedings Library (OPL)* **1262**, 1262 (2010).
- [11] N. Ishimatsu, T. Shichijo, Y. Matsushima, H. Maruyama, Y. Matsuura, T. Tsumuraya, T. Shishidou, T. Oguchi, N. Kawamura, M. Mizumaki, and K. Takemura, Hydrogen-induced modification of the electronic structure and magnetic states in Fe, Co, and Ni monohydrides, *Physical Review B* **86**, 104430 (2012).

- [12] C. Elsässer, J. Zhu, S. G. Louie, B. Meyer, M. Fähnle, and C. T. Chan, Ab initio study of iron and iron hydride: II. Structural and magnetic properties of close-packed Fe and FeH, *Journal of Physics: Condensed Matter* **10**, 5113 (1998).
- [13] T. Matsuoka, N. Hirao, Y. Ohishi, K. Shimizu, A. Machida, and K. Aoki, Structural and electrical transport properties of FeH<sub>x</sub> under high pressures and low temperatures, *High Pressure Research* **31**, 64 (2011).
- [14] Y. Shibazaki, E. Ohtani, H. Fukui, T. Sakai, S. Kamada, D. Ishikawa, S. Tsutsui, A. Q. Baron, N. Nishitani, N. Hirao, *et al.*, Sound velocity measurements in dhcp-FeH up to 70 GPa with inelastic X-ray scattering: Implications for the composition of the Earth's core, *Earth and Planetary Science Letters* **313**, 79 (2012).
- [15] N. Hirao, T. Kondo, E. Ohtani, K. Takemura, and T. Kikegawa, Compression of iron hydride to 80 GPa and hydrogen in the Earth's inner core, *Geophysical Research Letters* **31** (2004).
- [16] T. Tsumuraya, Y. Matsuura, T. Shishidou, and T. Oguchi, First-principles study on the structural and magnetic properties of iron hydride, *Journal of the Physical Society of Japan* **81**, 064707 (2012).
- [17] H. Gomi, Y. Fei, and T. Yoshino, The effects of ferromagnetism and interstitial hydrogen on the equation of states of hcp and dhcp FeH<sub>x</sub>: Implications for the Earth's inner core age, *American Mineralogist* **103**, 1271 (2018).
- [18] J. Ying, J. Zhao, W. Bi, E. E. Alp, Y. Xiao, P. Chow, G. Shen, and V. V. Struzhkin, Magnetic phase diagram of  $\epsilon'$ -FeH, *Physical Review B* **101**, 020405 (2020).
- [19] S. H. Lohaus, M. Heine, P. Guzman, C. M. Bernal-Choban, C. N. Saunders, G. Shen, O. Hellman, D. Broido, and B. Fultz, A thermodynamic explanation of the Invar effect, *Nature Physics* **19**, 1642 (2023).
- [20] P. Mohn, K. Schwarz, and D. Wagner, Magnetoelastic anomalies in Fe-Ni invar alloys, *Physical Review B* **43**, 3318 (1991).
- [21] L. Dubrovinsky, N. Dubrovinskaia, I. A. Abrikosov, M. Vennström, F. Westman, S. Carlson, M. van Schilfgaarde, and B. Johansson, Pressure-induced invar effect in Fe-Ni alloys, *Physical Review Letters* **86**, 4851 (2001).
- [22] T. Yokoyama and K. Eguchi, Anisotropic thermal expansion and cooperative Invar and anti-Invar effects in Mn alloys, *Physical Review Letters* **110**, 075901 (2013).

- [23] N. Ishimatsu, S. Iwasaki, M. Kousa, S. Kato, N. Nakajima, N. Kitamura, N. Kawamura, M. Mizumaki, S. Kakizawa, R. Nomura, T. Irifune, and H. Sumiya, Elongation of Fe-Fe atomic pairs in the Invar alloy Fe<sub>65</sub>Ni<sub>35</sub>, *Physical Review B* **103**, L220102 (2021).
- [24] E. Duman, M. Acet, T. Hülser, E. Wassermann, B. Rellinghaus, J. Itié, and P. Munsch, Large spontaneous magnetostrictive softening below the curie temperature of fe3c invar particles, *Journal of Applied Physics* **96**, 5668 (2004).
- [25] T. Katsura, K.-I. Funakoshi, A. Kubo, N. Nishiyama, Y. Tange, Y.-I. Sueda, T. Kubo, and W. Utsumi, A large-volume high-pressure and high-temperature apparatus for in situ X-ray observation, ‘SPEED-Mk. II’, *Physics of the Earth and Planetary Interiors* **143**, 497 (2004).
- [26] See Supplemental Material for the experimental and modeling details.
- [27] Y. Seto, Development of a software suite on x-ray diffraction experiments, *The Review of high pressure science and technology* **20**, 269 (2010).
- [28] Y. Seto, PDIndexer, <https://github.com/seto77/PDIndexer/>.
- [29] T. Takahashi and W. A. Bassett, High-pressure polymorph of iron, *Science* **145**, 483 (1964).
- [30] A. Georges, G. Kotliar, W. Krauth, and M. J. Rozenberg, Dynamical mean-field theory of strongly correlated fermion systems and the limit of infinite dimensions, *Review of Modern Physics* **68**, 13 (1996).
- [31] G. Kotliar, S. Y. Savrasov, K. Haule, V. S. Oudovenko, O. Parcollet, and C. A. Marianetti, Electronic structure calculations with dynamical mean-field theory, *Review of Modern Physics* **78**, 865 (2006).
- [32] S. V. Vonsovskii, M. I. Katsnel’son, and A. V. Trefilov, Localized and itinerant behavior of electrons in metals, *The Physics of Metals and Metallography* **76**, 247 (1993).
- [33] A. I. Lichtenstein, M. I. Katsnelson, and G. Kotliar, Finite-temperature magnetism of transition metals: An ab initio dynamical mean-field theory, *Physical Review Letters* **87**, 067205 (2001).
- [34] A. A. Katanin, A. I. Poteryaev, A. V. Efremov, A. O. Shorikov, S. L. Skornyakov, M. A. Korotin, and V. I. Anisimov, Orbital-selective formation of local moments in  $\alpha$ -iron: First-principles route to an effective model, *Physical Review B—Condensed Matter and Materials Physics* **81**, 045117 (2010).
- [35] I. Leonov, A. I. Poteryaev, V. I. Anisimov, and D. Vollhardt, Electronic correlations at the  $\alpha$ - $\gamma$  structural phase transition in paramagnetic iron, *Physical Review Letters* **106**, 106405

- (2011).
- [36] L. V. Pourovskii, T. Miyake, S. I. Simak, A. V. Ruban, L. Dubrovinsky, and I. A. Abrikosov, Electronic properties and magnetism of iron at the earth's inner core conditions, *Physical Review B—Condensed Matter and Materials Physics* **87**, 115130 (2013).
  - [37] K. Haule, Quantum Monte Carlo impurity solver for cluster dynamical mean-field theory and electronic structure calculations with adjustable cluster base, *Physical Review B* **75**, 155113 (2007).
  - [38] P. Blaha, K. Schwarz, G. K. H. Madsen, D. Kvasnicka, J. Luitz, R. Laskowski, F. Tran, and L. D. Marks, WIEN2k: An augmented plane wave plus local orbitals program for calculating crystal properties (Vienna University of Technology, Austria, 2018).
  - [39] J. P. Perdew, K. Burke, and M. Ernzerhof, Generalized gradient approximation made simple, *Physical Review Letters* **77**, 3865 (1996).
  - [40] Q. Han, T. Birol, and K. Haule, Phonon softening due to melting of the ferromagnetic order in elemental iron, *Physical Review Letters* **120**, 187203 (2018).
  - [41] P. Werner, A. Comanac, L. De'Medici, M. Troyer, and A. J. Millis, Continuous-time solver for quantum impurity models, *Physical Review Letters* **97**, 076405 (2006).
  - [42] H. Saitoh, A. Machida, R. Iizuka-Oku, T. Hattori, A. Sano-Furukawa, K.-I. Funakoshi, T. Sato, S.-I. Orimo, and K. Aoki, Crystal and Magnetic Structures of Double Hexagonal close-packed iron Deuteride, *Scientific reports* **10**, 1 (2020).
  - [43] C. Kittel and P. McEuen, *Introduction to Solid State Physics* (John Wiley & Sons, 2018).
  - [44] E. Wohlfarth, Thermodynamic aspects of itinerant electron magnetism, *Physica B+ C* **91**, 305 (1977).
  - [45] M. Shiga, Magnetism and spin fluctuations of laves phase manganese compounds, *Physica B+ C* **149**, 293 (1988).
  - [46] V. Antonov, K. Cornell, V. Fedotov, A. Kolesnikov, E. Ponyatovsky, V. Shiryayev, and H. Wipf, Neutron diffraction investigation of the dhcp and hcp iron hydrides and deuterides, *Journal of Alloys and Compounds* **264**, 214 (1998).
  - [47] A. Machida, H. Saitoh, H. Sugimoto, T. Hattori, A. Sano-Furukawa, N. Endo, Y. Katayama, R. Iizuka, T. Sato, M. Matsuo, S.-I. Orimo, and K. Aoki, Site occupancy of interstitial deuterium atoms in face-centred cubic iron, *Nature Communications* **5**, 5063 (2014).

- [48] A. Machida, H. Saitoh, T. Hattori, A. Sano-Furukawa, K.-I. Funakoshi, T. Sato, S.-I. Orimo, and K. Aoki, Hexagonal close-packed iron hydride behind the conventional phase diagram, *Scientific Reports* **9**, 1 (2019).
- [49] V. E. Antonov, V. M. Gurev, V. I. Kulakov, M. A. Kuzovnikov, I. A. Sholin, and V. Y. Zuykova, Solubility of deuterium and hydrogen in fcc iron at high pressures and temperatures, *Physical Review Materials* **3**, 113604 (2019).
- [50] A. Belozеров and V. Anisimov, Coulomb interaction parameters in bcc iron: an LDA+ DMFT study, *Journal of Physics: Condensed Matter* **26**, 375601 (2014).
- [51] A. Belozеров, A. Katanin, and V. Anisimov, Momentum-dependent susceptibilities and magnetic exchange in bcc iron from supercell dynamical mean-field theory calculations, *Physical Review B* **96**, 075108 (2017).
- [52] L. Pourovskii, J. Mravlje, M. Pozzo, and D. Alfe, Electronic correlations and transport in iron at Earth's core conditions, *Nature Communications* **11**, 4105 (2020).
- [53] H. Saitoh, A. Machida, H. Sugimoto, T. Yagi, and K. Aoki, P–V–T relation of the Fe–H system under hydrogen pressure of several gigapascals, *Journal of Alloys and Compounds* **706**, 520 (2017).
- [54] J. Nylén, T. Sato, E. Soignard, J. L. Yarger, E. Stoyanov, and U. Häussermann, Thermal decomposition of ammonia borane at high pressures, *The Journal of Chemical Physics* **131** (2009).
- [55] V. Antonov, B. Bulychev, V. Fedotov, D. Kapustin, V. Kulakov, and I. Sholin,  $\text{Nh}_3\text{bh}_3$  as an internal hydrogen source for high pressure experiments, *International Journal of Hydrogen Energy* **42**, 22454 (2017).
- [56] M. Matsui, Y. Higo, Y. Okamoto, T. Irifune, and K.-I. Funakoshi, Simultaneous sound velocity and density measurements of NaCl at high temperatures and pressures: Application as a primary pressure standard, *American Mineralogist* **97**, 1670 (2012).